Improved performance of organic light-emitting diodes with MoO₃ interlayer by oblique angle deposition

S.W. Liu,[1] Y. Divayana,[1] X.W. Sun,[1,2,*] Y. Wang,[1]
K.S. Leck,[1] and H.V. Demir[1,3,4,5,6]

[1]*School of Electrical and Electronic Engineering, Nanyang Technological University, Nanyang Avenue, 639798, Singapore*
[2]*Department of Applied Physics, College of Science, Tianjin University, Tianjin 300072, China*
[3]*School of Physical and Mathematical Sciences, Nanyang Technological University, Nanyang Avenue, 639798, Singapore*
[4]*Department of Electrical and Electronic Engineering, Department of Physics, Bilkent University, Bilkent, Ankara 06800, Turkey*
[5]*Optical Society of America, 2010 Massachusetts Avenue, NW, Washington, D.C. 20036, USA*
[6]*hvdemir@ntu.edu.sg*
**exwsun@ntu.edu.sg*

Abstract: We fabricated and demonstrated improved organic light emitting diodes (OLEDs) in a thin film architecture of indium tin oxide (ITO)/ molybdenum trioxide (MoO₃) (20 nm)/ N,N'-Di(naphth-2-yl)-N,N'-diphenyl-benzidine (NPB) (50 nm)/ tris-(8-hydroxyquinoline) (Alq₃) (70 nm)/ Mg:Ag (200 nm) using an oblique angle deposition technique by which MoO₃ was deposited at oblique angles (θ) with respect to the surface normal. It was found that, without sacrificing the power efficiency of the device, the device current efficiency and external quantum efficiency were significantly enhanced at an oblique deposition angle of $\theta = 60°$ for MoO₃.

©2011 Optical Society of America

References and links

1. S. R. Forrest, "The path to ubiquitous and low-cost organic electronic appliances on plastic," Nature **428**(6986), 911–918 (2004).
2. C. W. Tang, and S. A. Vanslyke, "Organic electroluminescent diodes," Appl. Phys. Lett. **51**(12), 913–915 (1987).
3. C. C. Wu, C. I. Wu, J. C. Sturm, and A. Kahn, "Surface modification of indium tin oxide by plasma treatment: An effective method to improve the efficiency, brightness, and reliability of organic light emitting devices," Appl. Phys. Lett. **70**(11), 1348–1350 (1997).
4. C. Ganzorig, K. J. Kwak, K. Yagi, and M. Fujihira, "Fine tuning work function of indium tin oxide by surface molecular design: Enhanced hole injection in organic electroluminescent devices," Appl. Phys. Lett. **79**(2), 272–274 (2001).
5. S. A. Van Slyke, C. H. Chen, and C. W. Tang, "Organic electroluminescent devices with improved stability," Appl. Phys. Lett. **69**(15), 2160–2162 (1996).
6. S. Tokito, K. Noda, and Y. Taga, "Metal oxides as a hole-injecting layer for an organic electroluminescent device," J. Phys. D Appl. Phys. **29**(11), 2750–2753 (1996).
7. I. H. Hong, M. W. Lee, Y. M. Koo, H. Jeong, T. S. Kim, and O. K. Song, "Effective hole injection of organic light-emitting diodes by introducing buckminsterfullerene on the indium tin oxide anode," Appl. Phys. Lett. **87**(6), 063502 (2005).
8. J. Kido, and T. Matsumoto, "Bright organic electroluminescent devices having a metal-doped electron-injecting layer," Appl. Phys. Lett. **73**(20), 2866–2868 (1998).
9. T. Matsushima, and C. Adachi, "Enhanced hole injection and transport in molybdenum-dioxide-doped organic hole-transporting layers," J. Appl. Phys. **103**(3), 034501 (2008).
10. H. You, Y. F. Dai, Z. Q. Zhang, and D. G. Ma, "Improved performances of organic light-emitting diodes with metal oxide as anode buffer," J. Appl. Phys. **101**(2), 026105 (2007).
11. H. Kanno, R. J. Holmes, Y. Sun, S. Kena-Cohen, and S. R. Forrest, "White stacked electrophosphorescent organic light-emitting devices employing MoO3 as a charge-generation layer," Adv. Mater. (Deerfield Beach Fla.) **18**(3), 339–342 (2006).

12. T. Matsushima, G. H. Jin, and H. Murata, "Marked improvement in electroluminescence characteristics of organic light-emitting diodes using an ultrathin hole-injection layer of molybdenum oxide," J. Appl. Phys. **104**(5), 054501 (2008).
13. H. M. Zhang, Y. F. Dai, D. G. Ma, and H. Zhang, "High efficiency tandem organic light-emitting devices with Al/WO3/Au interconnecting layer," Appl. Phys. Lett. **91**(12), 123504 (2007).
14. X.-Y. Jiang, Z.-L. Zhang, J. Cao, M. A. Khan, Khizar-ul-Haq, and W.-Q. Zhu, "White OLED with high stability and low driving voltage based on a novel buffer layer MoOx," J. Phys. D Appl. Phys. **40**(18), 5553–5557 (2007).
15. H. Kanno, N. C. Giebink, Y. R. Sun, and S. R. Forrest, "Stacked white organic light-emitting devices based on a combination of fluorescent and phosphorescent emitters," Appl. Phys. Lett. **89**(2), 023503 (2006).
16. R. Satoh, S. Naka, M. Shibata, H. Okada, H. Onnagawa, T. Miyabayashi, and T. Inoue, "Top-emission organic light-emitting diodes with ink-jet printed self-aligned emission zones," Jpn. J. Appl. Phys. **45**(3A), 1829–1831 (2006).
17. S. T. Lee, Y. M. Wang, X. Y. Hou, and C. W. Tang, "Interfacial electronic structures in an organic light-emitting diode," Appl. Phys. Lett. **74**(5), 670–672 (1999).
18. E. Tutiŝ, D. Berner, and L. Zuppiroli, "Internal electric field and charge distribution in multilayer organic light-emitting diodes," J. Appl. Phys. **93**(8), 4594–4602 (2003).
19. Y. Zou, Z. B. Deng, Z. Y. Lv, Z. Chen, D. H. Xu, Y. L. Chen, Y. H. Yin, H. L. Du, and Y. S. Wang, "Reduction of driving voltage in organic light-emitting diodes with molybdenum trioxide in CuPc/NPB interface," J. Lumin. **130**(6), 959–962 (2010).
20. T. Matsushima, Y. Kinoshita, and H. Murata, "Formation of Ohmic hole injection by inserting an ultrathin layer of molybdenum trioxide between indium tin oxide and organic hole-transporting layers," Appl. Phys. Lett. **91**(25), 253504 (2007).
21. M. M. Hawkeye, and M. J. Brett, "Glancing angle deposition: fabrication, properties, and applications of micro- and nanostructured thin films," J. Vac. Sci. Technol. A **25**(5), 1317–1335 (2007).
22. B. J. Chen, X. W. Sun, B. K. Tay, L. Ke, and S. J. Chua, "Improvement of efficiency and stability of polymer light-emitting devices by modifying indium tin oxide anode surface with ultrathin tetrahedral amorphous carbon film," Appl. Phys. Lett. **86**(6), 063506 (2005).
23. J. X. Guo, Z. Sun, B. K. Tay, and X. W. Sun, "Field emission from modified nanocomposite carbon films prepared by filtered cathodic vacuum arc at high negative pulsed bias," Appl. Surf. Sci. **214**(1–4), 351–358 (2003).
24. E. Ito, H. Oji, H. Ishii, K. Oichi, Y. Ouchi, and K. Seki, "Interfacial electronic structure of long-chain alkane/metal systems studied by UV-photoelectron and metastable atom electron spectroscopies," Chem. Phys. Lett. **287**(1–2), 137–142 (1998).
25. C. Hosokawa, H. Tokailin, H. Higashi, and T. Kusumoto, "Transient-behavior of organic thin-film electroluminescence," Appl. Phys. Lett. **60**(10), 1220–1222 (1992).
26. W. J. Shin, J. Y. Lee, J. C. Kim, T. H. Yoon, T. S. Kim, and O. K. Song, "Bulk and interface properties of molybdenum trioxide-doped hole transporting layer in organic light-emitting diodes," Org. Electron. **9**(3), 333–338 (2008).
27. H. Aziz, Z. D. Popovic, N. X. Hu, A. M. Hor, and G. Xu, "Degradation mechanism of small molecule-based organic light-emitting devices," Science **283**(5409), 1900–1902 (1999).
28. J. Kalinowski, L. C. Palilis, W. H. Kim, and Z. H. Kafafi, "Determination of the width of the carrier recombination zone in organic light-emitting diodes," J. Appl. Phys. **94**(12), 7764–7767 (2003).

1. Introduction

Organic light-emitting diodes (OLEDs) are regarded as very promising for the next generation flat panel display technology thanks to their favorable properties of self-emission, low temperature fabrication, low cost, wide viewing angle, flexible form and high contrast [1]. Beginning with the demonstration of the first bilayer OLED in 1987 [2], this class of optoelectronic devices has been intensively studied and various attempts have been made to improve their performances, e.g., by electrode modification [3,4], insertion of a buffer layer between the metal electrode and the organic layer [5–7], and doping [8,9].

Recently, molybdenum trioxide (MoO_3) has been widely investigated as a hole injection layer (HIL) material to reduce the operating voltage and improve the device performance and lifetime [10–16]. However, it is well known that, for a typical green-emitting OLED, holes experience a smaller injection barrier compared to that of electrons [17], and the hole mobility in the hole transport layer (HTL) is an order of magnitude higher than that of the electron in the electron transport layer (ETL) [18]. Therefore, there exists an intrinsic electron-hole imbalance in these devices, and this decreases their efficiency. Although the insertion of MoO_3 buffer layer results in an enhanced hole injection and improved device stability, this simultaneously substantially deteriorates the electron-hole balance, which correspondingly reduces the current and quantum efficiencies of the resulting devices [12,19].

In this letter, we developed an oblique angle deposition technique of MoO_3 to fabricate our OLEDs. Systematically varying the angle of deposition (θ) with respect to the surface normal, we found that the device current efficiency and external quantum efficiency (EQE) are significantly increased for $\theta = 60°$, without sacrificing the power efficiency.

2. Experimental details

In this study, we used MoO_3 as HIL, N,N'-Di(naphth-2-yl)-N,N'-diphenyl-benzidine (NPB) as HTL, tris-(8-hydroxyquinoline) (Alq_3) as emissive and electron transport layers, and transparent indium tin oxide (ITO) and Mg:Ag as anode and cathode, respectively. The device structure consisted of ITO/ MoO_3 (20 nm deposited at various θ)/ NPB (50 nm)/ Alq_3 (70 nm)/ Mg:Ag (200 nm), where θ is the tilt angle of ITO glass substrate with respect to the sample holder, or equivalently, the angle of deposition with respect to the surface normal of the substrate [the oblique deposition angle, as shown in the inset of Fig. 1(b)]. When MoO_3 was deposited, the substrates were oriented at the targeted angle θ, given the fixed vertical material evaporation in the vacuum chamber. For a parametric study of θ, only MoO_3 layers were deposited at various oblique angles of θ, while the rest of organic and metal layers was laid down in the surface normal configuration (i.e., when the substrates were placed parallel to the sample holder and perpendicular to the evaporation direction). The deposition rate was 0.1 nm/s for MoO_3, 0.1-0.2 nm/s for NPB and Alq_3, 0.3-0.4 nm/s for the cathode, while the system vacuum was kept under 5×10^{-4} Pa during the whole deposition process. Here θ was set to 0° (for the surface normal configuration as a negative control device), and 30°, 45°, 60°, and 80° for the systematic study.

The device fabrication is briefly introduced as follows. The ITO glass (20Ω/□) was first cleaned by a routine procedure that includes ultrasonication in acetone and ethanol, and subsequent rinsing in de-ionized water. After ITO glass was dried in an oven, an oxygen plasma was used to remove the excess moisture and residual contaminants from the cleaned substrate. Then the ITO substrates were transferred into the deposition chamber for thin film deposition. The deposition chamber contains 10 crucibles, holding up to 10 different sources, each of which is heated by a tantalum heater. There were three sets of shutters working together to achieve large area uniformity and abrupt interface. Right on top of each crucible one set of the shutters was placed, through which the open/close sequence controls the material deposition, while the big shutters between the crucibles and the substrates are used in combination with the small ones under each substrate, to isolate the substrate from the evaporated material. The deposition rate and thickness are monitored by a 6 MHZ gold crystal sensor and a quartz oscillator combined with a frequency meter; the crystal sensor is mounted in the center right below the substrate holders, which can be rotated at an adjustable speed. The electroluminescence (EL) spectra of the fabricated devices were measured using a PR650 Spectra Scan spectrometer, while the luminance-current density-voltage (L-J-V) characteristics were obtained simultaneously, by connecting the spectrometer to a programmable Keithley 236 source measurement unit. All measurements were carried out at room temperature under ambient conditions without encapsulation.

3. Results and discussion

Figures 1(a) and 1(b) present the current density versus voltage (J-V) and luminance versus current density (L-J) characteristics for the control device ($\theta = 0°$) as well as the parametric set of devices with MoO_3 deposited at $\theta = 30°$, 45°, 60° and 80°, respectively. The inset of Fig. 1(a) shows the applied voltage for the above mentioned deposition angles at a fixed current density of 35 mA/cm^2. It can be seen that the device with MoO_3 deposited at $\theta = 60°$ yields the largest operating voltage compared to the rest, while the operating voltage for the other devices with MoO_3 deposited at $\theta = 30°$, 45° and 80° is slightly reduced at the same current density compared to the control device and gets closer to that of the control device at high current density. In Fig. 1(b), the highest luminance occurs for the device with MoO_3 deposited at $\theta = 60°$.
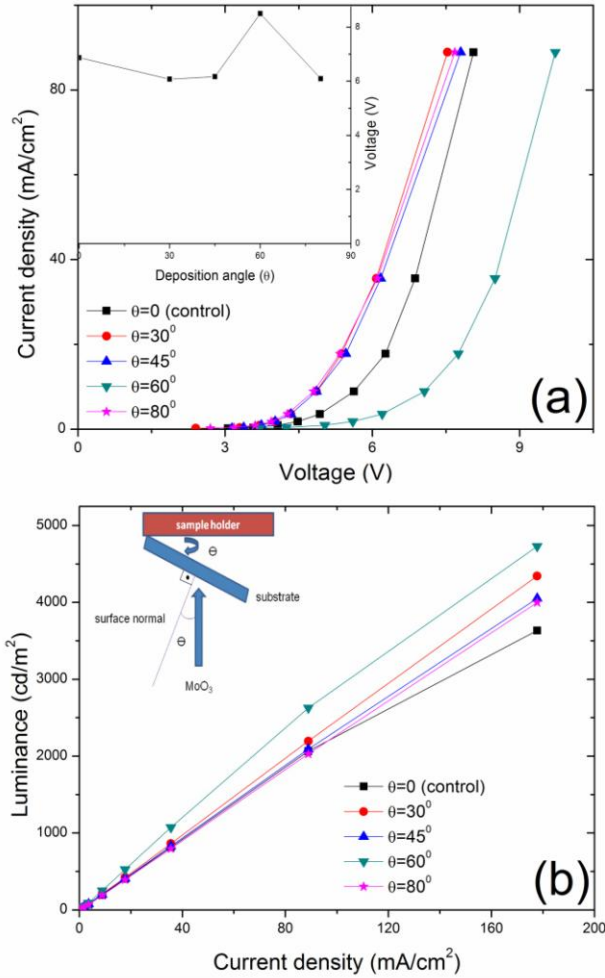
Fig. 1. (a) Current density *vs.* voltage and (b) luminance *vs.* current density for the ITO/MoO$_3$(θ)/NPB/Alq$_3$/Mg:Ag structures parameterized with respect to θ, the deposition angle of MoO$_3$. The inset in (a) shows the applied voltage *vs.* deposition angle at a current density of 35 mA/cm^2. The inset in (b) illustrates the orientation of the substrate placed at a deposition angle (θ) with respect to the surface normal during MoO$_3$ evaporation.

It is clear that the resultant J-V curve is not caused by the thickness variation of deposited MoO$_3$ layer because the device at θ = 60° would otherwise have an enhanced hole injection. Since the deposited MoO$_3$ layer thickness in the substrate surface normal direction shall be the nominal thickness (i.e., 20 nm) multiplied by cos(θ), where θ is the angle between the substrate surface normal and vertical direction, this theoretically gives 20 nm, 17.3 nm, 14.1 nm, 10 nm and 3.5 nm for an oblique deposition angle of 0°, 30°, 45°, 60° and 80°, respectively. Matsushima *et al.* [12,20] reported that when the deposited MoO$_3$ thickness between the ITO and an organic is between 2 and 20 nm, the J-V characteristics are not much affected; we verified this finding by fabricating "hole only" devices consisting of ITO/ MoO$_3$ (X nm)/ NPB (100 nm)/ Mg:Ag (200 nm), where X was set to 3.5 nm, 10 nm, 14.1 nm, 17.3 nm and 20 nm, while MoO$_3$ was deposited at 0° for all samples. The J-V characteristics of these "hole only" devices are shown in the inset of Fig. 2(a), from which we can see that the resulting hole injection characteristics did not significantly differ when MoO$_3$ thickness was varied from 3.5 to 20 nm. Therefore, the possible device fabrication parameter affecting the

performance is the oblique flux angle, which affects the surface morphology of the fabricated devices.

Next the surface morphology of MoO_3 films deposited on ITO glass substrate at different angles was investigated by atomic force microscopy (AFM). The AFM images were obtained over an area of 2 μm × 2 μm for the MoO_3 films deposited at different angles of 0°, 30°, 45°, 60° and 80°. The morphology of the samples with MoO_3 deposited at angles other than 60° exhibits many sharp spikes and their roughness is larger compared with that of the MoO_3 film deposited at 60°. The surface roughness data are summarized in Table 1. The surface of the MoO_3 film deposited at 60° shows the smallest roughness and is more uniform compared with others. This is probably due to the ease of ITO pits filling at the oblique angle of 60°. The non-monotonic behavior of the surface roughness for different deposition angles is due to the competition between surface diffusion and ballistic shadowing [21]. According to Hawkeye *et al.* [21], ballistic shadowing leads to the preferential growth of the tallest columns inclined towards the source, producing a rougher surface. Surface diffusion, which is inversely proportional to the deposition rate, causes the deposited atoms/molecules to redistribute, promoting a smoother surface. Extinction occurs if the small columns fall into the "shadow" of the larger neighboring columns, then the small columns will no longer receive any vapor flux. At oblique angle θ, the amount of vapor flux towards one unit surface area is decreased by cos θ, i.e. the surface deposition rate is decreased with increasing θ. At a low oblique deposition angle, the ballistic shadowing effect and the surface diffusion are comparable, leading to a surface with roughness similar to that of the normal deposition. When the oblique angle is increased, the surface deposition rate is decreased significantly, thus, the surface diffusion is greatly enhanced, which overtakes the effect of ballistic shadowing, resulting in a more uniform surface with smaller roughness. However, at a large deposition angle (larger than 60° in the experiment), ballistic shadowing effect becomes strong, which eventually leads to extinction, the smaller columns which fall into the "shadow" of the larger neighboring columns can no longer receive any incoming MoO_3 flux, and surface diffusion is insufficient to fill out the shadows, resulting in a rougher surface. By ploting the surface roughness as a function of the deposition angle (inset of Fig. 3) and comparing the plot with the inset of Fig. 1(a), which shows the plot of the applied voltage with respect to the deposition angle, we observed that when the film surface is rougher and less uniform (Table 1), the corresponding applied voltage is smaller. Although at 45°, the RMS (Root Mean Square) roughness is 2.3 ± 0.1 nm, the peak to peak roughness is very large (39.1 ± 1.5 nm), signifying a non-uniform surface.

Table 1. Summary of Surface Roughness of MoO₃ Films Deposited at Different Angles

Deposition Angle	Peak-to-Peak Roughness (nm)	RMS Roughness (nm)	Mean Roughness (nm)
0°	36.7 ± 1.0	2.7 ± 0.5	1.7 ± 0.2
30°	41.4 ± 1.5	2.8 ± 0.5	1.9 ± 0.4
45°	39.1 ± 1.5	2.3 ± 0.4	1.4 ± 0.1
60°	19.9 ± 1.5	1.6 ± 0.1	1.1 ± 0.1
80°	32.6 ± 1.0	4.0 ± 0.3	3.2 ± 0.4

The reduced voltage for a rougher and non-uniform surface is caused by the enhanced hole injection owing to possible nanostructured interface formation resulting from the rough surface, which is similar to the case of enhanced field emission of nanostructured films [22,23]. At the deposition angle of 60°, the MoO₃ surface is much more uniform, we suggest that the interfacial dipole layer (IDL) formed between MoO₃ and NPB is much stronger compared with that of the devices deposited at other angles because the ionization potential (IP) critically depends on the surface morphology [17], while the IDL formed may impede hole injection at the MoO₃/organic interface [24].

It is well known that the hole mobility in NPB is several orders of magnitude larger than that of the electron in Alq₃ [25], and for an OLED composed of ITO/HIL/NPB/Alq₃/Mg:Ag, the hole injection barrier (1.7 eV) is smaller than the electron injection barrier (2.0 eV) [17]. Therefore, there is an intrinsic electron-hole imbalance in such typical green emitting devices. However, the impedance of the hole injection from ITO anode to NPB due to a strong IDL formed at the MoO₃ ($\theta = 60°$)/organic interface may alleviate the problem of electron-hole imbalance, which is good for higher device efficiencies.

Figures 2(a) and 2(b) show the current efficiency and power efficiency versus current density, respectively. In Fig. 2(a), at a current density of 35 mA/cm², the current efficiencies for the devices with MoO₃ deposited at $\theta = 0°$ (control), 30°, 45°, 60° and 80° are found to be 2.28, 2.42, 2.33, 3.02 and 2.24, respectively. This indicates an increase in efficiency for the device with $\theta = 60°$ compared to that of the control device, while the other devices with $\theta = 30°$, 45° and 80° have similar levels of current efficiency compared to the control device. Furthermore, we attribute the improved performance to the better electron-hole balance in the case of $\theta = 60°$. The power efficiency for the device with MoO₃ deposited at $\theta = 60°$, from Fig. 2(b), however, is comparable to (or slightly better than) that of the control device. This is due to the fact that the power efficiency is determined by both the EQE and device operating voltage [26], and the high EQE for the case of $\theta = 60°$ [inset of Fig. 2(b)] compensates for the effect of increased operating voltage caused by the impedance of hole injection. The resultant high EQE for $\theta = 60°$ is caused by a comparatively more balanced electron and hole concentration in the device. The decreased hole injection from the anode minimizes the hole leakage to the cathode; therefore, it reduces the formation of cationic Alq₃ [27], which is one of the main culprits of the decreased fluorescence efficiency and device stability. Moreover, the reduction of hole injection, according to Kalinowaski et al. [28], is equivalent to minimizing the carrier recombination to the transit time ratio (t_{rec}/t_t), which is inversely related to the quantum efficiency.
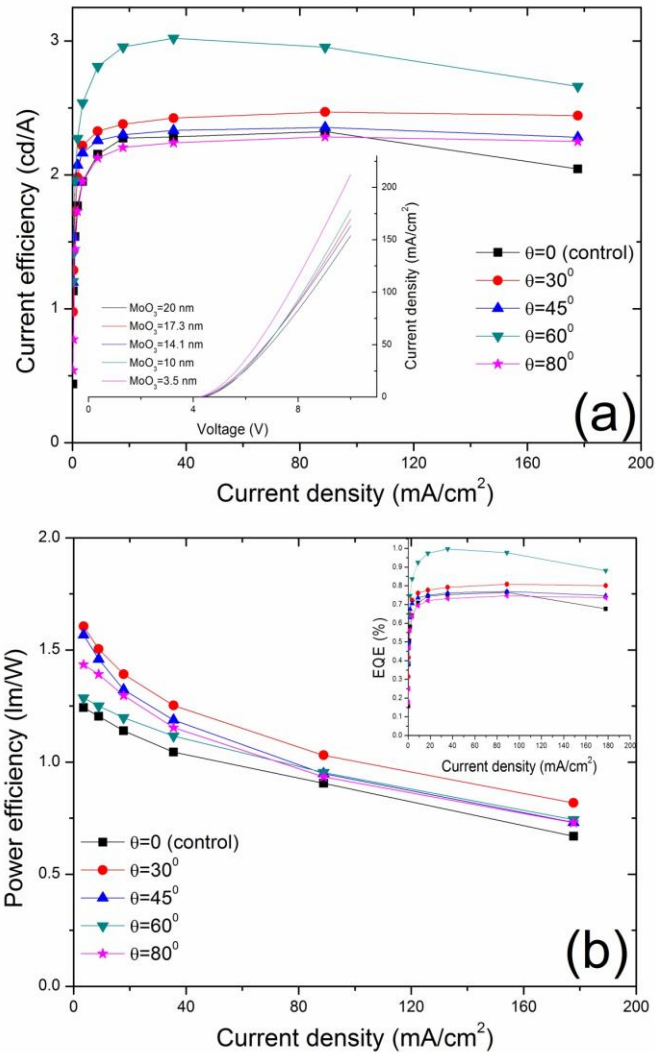
Fig. 2. (a) Current efficiency *vs.* current density and (b) power efficiency *vs.* current density for the ITO/MoO$_3$(θ)/NPB/Alq$_3$/Mg:Ag structures parameterized with respect to θ, the deposition angle of MoO$_3$. The inset in (a) shows the current density *vs.* voltage for the "hole only" devices with MoO$_3$ deposited at 0° with different film thickness of 3.5 nm, 10 nm, 14.1 nm, 17.3 nm and 20 nm. The inset in (b) shows the EQE *vs.* current density.

To verify the effect of MoO$_3$ film deposited at θ = 60° on the hole injection, we constructed 'hole only' devices with a thin-film structure of ITO /MoO$_3$ (20 nm deposited at θ) /NPB (100 nm) /Mg:Ag (excluding the Alq$_3$ ETL in the device). The large electron barrier at the Mg:Ag/NPB interface in this set of devices ensures that the electron concentration in the fabricated devices is negligible compared to that of the holes. Figure 3 depicts the J-V characteristics for the resulting 'hole only' devices, from which we can observe clearly that the operating voltage for the device with MoO$_3$ deposited at θ = 60° is increased compared to that of devices with MoO$_3$ deposited at other angles. Therefore, the deposition angle of MoO$_3$, θ, which influences the final surface morphology of the fabricated devices, can serve as a control parameter to tune the hole injection.

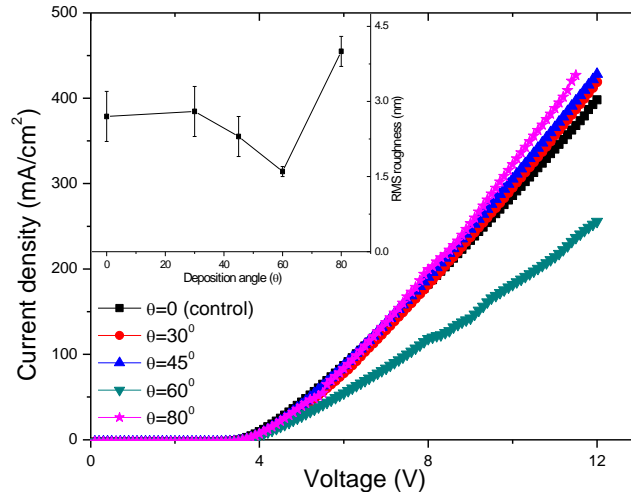Fig. 3. Current density *vs.* voltage characteristics of the 'hole only' devices (ITO/MoO$_3$(θ)/NPB/Mg:Ag structures) parameterized with respect to θ, the deposition angle of MoO$_3$. The inset shows the RMS roughness *vs.* deposition angle.

4. Conclusion

In summary, we systematically studied the effect of an oblique angle deposition of MoO$_3$ on the performance of organic light-emitting diodes with a structure of indium tin oxide (ITO)/ molybdenum trioxide (MoO$_3$) (θ)/ N,N'-Di(naphth-2-yl)-N,N'-diphenyl-benzidine (NPB/ tris-(8-hydroxyquinoline) (Alq$_3$)/ Mg:Ag. At the optimized deposition angle of 60°, we found that the decreased hole injection is caused by the stronger interfacial dipole layer between MoO$_3$ and NPB associated with the surface morphology. It is inferred that this behavior is caused by the stronger interfacial dipole layer which may be formed associated with the surface morphology. The effects of the reduced hole injection on the device performance are discussed. Finally, it is verified from the 'hole only' devices (without the electron transport layer) that the device with MoO$_3$ deposited at θ = 60° shows decreased hole injection behavior. The device current efficiency and external quantum efficiency were found to be significantly enhanced for θ = 60° while maintaining the power efficiency of the device.

Acknowledgments